PCCP

Synthesis of cubic PtPd alloy nanoparticles as an anode electrocatalyst for methanol and formic acid oxidation reactions

Journal:	*Physical Chemistry Chemical Physics*
Manuscript ID:	CP-COM-02-2015-000892.R1
Article Type:	Communication
Date Submitted by the Author:	26-Feb-2015

Complete List of Authors:	Lee, Jin-Yeon; Soongsil University, Chemical Engineering Kwak, Da-Hee; Soongsil University, Chemical Engineering Lee, Young-Woo; Soongsil University, Chemical and Environmental Engineering Lee, Seul; Soongsil University, Chemical Engineering Park, Kyung-Won; Soongsil University, Chemical Engineering

Journal Name

RSCPublishing

ARTICLE

Synthesis of cubic PtPd alloy nanoparticles as an anode electrocatalyst for methanol and formic acid oxidation reactions

0Cite this: DOI: 10.1039/x0xx00000x

Jin-Yeon Lee,[a] Da-Hee Kwak,[a] Young-Woo Lee,[a,b] Seul Lee,[a] Kyung-Won Park[a,*]

Received 00th January 2012,
Accepted 00th January 2012

DOI: 10.1039/x0xx00000x

www.rsc.org/

The electrocatalytic properties for electro-oxidation reactions of shape-controlled Pt-based catalysts have been improved by alloying with 2nd elements. In this study, we demonstrate cubic PtPd alloy nanoparticles synthesized using a thermal decomposition method. The cubic PtPd nanoparticles exhibit a homogeneous distribution of alloy nanostructure in the presence of Pt and Pd metallic phases. The improved electrocatalytic activity for the electro-oxidation reactions of methanol and formic acid as chemical fuels might be attributed to the cubic alloy nanostructure. Furthermore, the cubic PtPd alloy nanoparticles as an electrocatalyst exhibit an excellent stability for electro-oxidation reactions.

1. Introduction

For methanol oxidation in direct methanol fuel cells (DMFCs), Pt and Pt-based catalysts are widely used as efficient anode catalysts especially in acid medium.[1-4] However, a critical problem with Pt-based catalysts is the CO poisoning effect during methanol electrooxidation reaction (MOR) in acid medium.[5,6] As illustrated in Fig. 1a, during the electrooxidation of methanol as a fuel in DMFCs, the methanol is oxidized to a CO-like intermediate that bonds strongly to a metallic catalyst surface, preventing the fuel adsorption, and the intermediate is then oxidized to CO_2.[7-9] Thus, many recent efforts have been made to overcome the CO poisoning effect, improve the electrocatalytic activity, and reduce the use of Pt on metallic catalysts by alloying Pt with other metals (e.g., Pd, Au, and Ru).[10-14] In particular, this results from the bifunctional mechanism of the other alloyed metals and the electronic effects in PtPd alloy catalysts with higher activity and better stability for MOR in comparison with pure Pt.[15]

The direct formic acid fuel cell (DFAFC) has been a promising electrochemical energy devices due to its high theoretical energy density and easier storage and handling than H_2 as a chemical fuel in fuel cells.[16-19] In DFAFC, formic acid as a fuel can facilitate both proton and electron transport at the anode region. Formic acid oxidation reaction (FAOR) on Pt catalyst follows a dual path mechanism (i.e. dehydrogenation and dehydration path) and adsorption of intermediate CO from the dehydration path retards its activity of oxidizing to CO_2 (Fig. 1b).[20,21] The elimination of the CO poisoning effect has been throughly attempted by alloying Pt with other metals or using a Pd based catalyst.[22] However, the structure and/or shape effect of Pt- or Pd-based anode nanostructure catalysts used in the DFAFC should still be considered for commercial applications.

Platinum nanoparticles (NPs) with elaborately controlled shapes such as cubes, tetrahedrons, octahedrons, and cuboctahedrons have exhibited unique catalytic properties for oxidation reactions in electrochemical power sources compared to polycrystalline NPs.[23-27] Since the exposed surfaces of the shape-controlled NPs can hold particular crystal planes, the selectivity and reactivity of Pt NPs in catalytic applications can be modulated by controlling the shape or morphology.[28-30] Thus, to improve their catalytic activity and stability, significant effort has been focused on the synthesis of Pt-based nanostructures for oxidation of methanol and formic acid as a fuel in fuel cells.[31,32] The advantages of shape-controlled Pt-based nanostructures are high surface-area-to-volume ratio, enhanced specific area and mass electrochemical activity, and the ease of control of reaction selectivity according to various reactants.[33,34] Recent advances in NP synthetic methodology have led to the formation of monodisperse metallic NPs to enhance activity for the oxidation of fuels such as hydrogen, formic acid, methanol, and ethanol in polymer electrolyte membrane fuel cell conditions.[35] In particular, it was reported that the higher reactivity of the oxidation reactions on the {100} facets of the cubic Pt-based catalysts than on the {111} and {110} facets might be attributed to the dominant direct pathway for the MOR and FAOR (Fig. 1c).[36] Here, we demonstrate a synthesis of cubic PtPd alloy NPs for enhanced MOR and

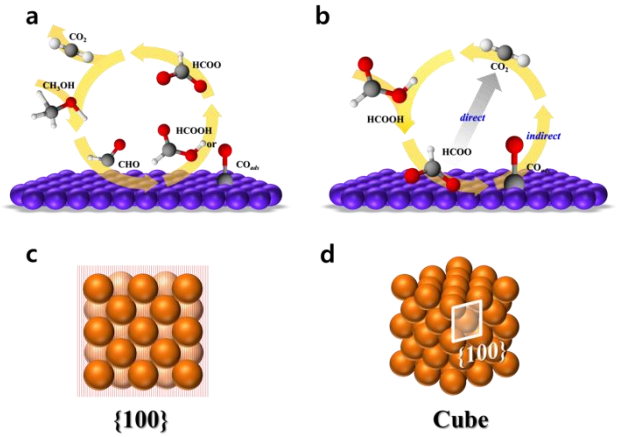

Fig. 1 Mechanism of (a) methanol and (b) formic acid oxidation reactions on the catalyst. (c) {100} surfaces of Pt-based catalysts with a face-centered cubic structure. (d) Cubic Pt-based nanostructure catalysts with dominant {100} facets.

FAOR using a thermal-decomposition method in the presence of $Mo(CO)_6$ (Fig. 1d). The NPs were examined for MOR/ FAOR catalysis in acidic electrolyte and oxidation conditions. The cubic PtPd alloy NPs showed highly improved activity and stability for both MOR and FAOR, serving as a promising candidate for the electro-oxidation of small organic molecules.

2. Experimental Methods

2.1. Synthesis of cubic PtPd alloy and cubic Pt NPs

Cubic PtPd NPs were prepared using a thermal decomposition method in the presence of $Mo(CO)_6$. A mixture solution of 6 ml oleylamine (70%, Aldrich), 2 ml oleic acid (65~88%, Aldrich), and 0.07 g $Mo(CO)_6$ (98%, Aldrich) was prepared under an N_2 atmosphere. The mixed solution was increased by 6 ^oC min^{-1} to 250 ^oC and kept for 10 min. A metal salt solution of 4.5 mM 0.0177 g $Pt(acac)_2$ (97%, Aldrich), 1.5 mM 0.0046 g $Pd(acac)_2$ (95%, Aldrich) and 2 ml oleylamine was added to the mixed solution and then maintained at 250 ^oC for 2 h. All resulting colloidal solutions were rapidly cooled down by pouring into 75 ml n-hexane (95%, SAMCHUN). The resulting products were collected and washed several times with ethanol (95%, SAMCHUN) and acetone (99.7%, SAMCHUN) using centrifugation. To completely remove the remaining surfactant after the reaction, the products were kept in a 30 ml acetic acid solution (99.7%, SAMCHUN) at 80 ^oC for 12 h. The final products were washed with ethanol and acetone several times and dried in an oven at 50 ^oC.

For comparison, cubic Pt NPs were prepared using a thermal decomposition method in the presence of $Mo(CO)_6$. A mixture solution of 6 ml oleylamine (70%, Aldrich), 2 ml oleic acid (65~88%, Aldrich), and 0.07 g $Mo(CO)_6$ (98%, Aldrich) was prepared under an N_2 atmosphere. The mixed solution was increased by 6 ^oC min^{-1} to 250 ^oC and kept for 10 min. A metal salt solution of 6.0 mM 0.0236 g $Pt(acac)_2$ (97%, Aldrich) and 2 ml oleylamine was added to the mixed solution and then maintained at 250 ^oC for 2 h.

All resulting colloidal solutions were rapidly cooled down by pouring into 75 ml n-hexane (95%, SAMCHUN). The resulting products were collected and washed several times with ethanol (95%, SAMCHUN) and acetone (99.7%, SAMCHUN) using centrifugation. To completely remove the remaining surfactant after the reaction, the products were maintained in a 30 ml acetic acid solution (99.7%, SAMCHUN) at 80 ^oC for 12 h. The final products were washed with ethanol and acetone several times and dried in an oven at 50 ^oC.

2.2. Synthesis of Polycrystalline PtPd alloy NPs

The polycrystalline PtPd alloy NPs (denoted as poly-PtPd) were prepared by simultaneously reducing Pd and Pt salts using a borohydride reduction method. A solution of 1.5 mM 0.061 g $H_2PtCl_6 \cdot H_2O$ (100%, Aldrich) and 0.5 mM 0.0088 g $PdCl_2$ (99.9%, Aldrich) was dissolved in 80 ml de-ionized water with vigorous stirring for 2 h and then 2.4 mM $NaBH_4$ solution as a reducing agent was added to the metal salt solution. The final product was washed with ethanol and acetone several times and dried in an oven at 50 ^oC.

2.3. Characterization of NPs

XRD patterns of the samples were obtained using a D2 PHASE SYSTEM, BRUKER with Cu K_α source (λ = 0.15406 nm) radiation at 30 kV and 10 mA in $2\theta = 20°$ to 80°. The size and morphology of the catalysts were analyzed using transmission electron microscopy (TEM) with a Tecnai G2 F30 system microscope operating at 300 kV. Energy dispersive X-ray (EDX) analysis of the samples was performed on a field emission transmission electron microscope (FE-TEM) (Tecnai G2 F30 system). TEM samples were prepared by placing drops of catalyst suspension dispersed in ethanol on a carbon-coated copper grid. X-ray photoelectron spectroscopy (XPS) (Thermo Scientific, K-Alpha) analysis was carried out with an Al K_α X-ray source of 1486.8 eV at a chamber pressure below 1×10^{-8} Torr and beam power of 200 W. All of the high resolution spectra were collected using a pass energy of 46.95 eV. The step size and time per step were chosen to be 0.025 eV and 100 ms, respectively. Both ends of the baseline were set sufficiently far apart, to avoid distorting the shape of the spectra, including their tails. A small variation of the range of the baseline did not affect the relative number of fitted species (less than 1%). The C 1s electron binding energy was referenced at 284.6 eV and a nonlinear least-squares curve-fitting program was employed with a Gaussian-Lorentzian production function.

The electrocatalytic properties were measured in a three-electrode cell using a potentiostat (Eco Chemie, AUTOLAB) at room temperature with a scan rate of 50 mV s^{-1}. Pt wire and Ag/AgCl (in 3 M KCl) were used as counter and reference electrodes, respectively. The glassy carbon working electrode was coated with 6.5 μL of catalyst ink prepared by mixing NPs and 10 mL de-ionized water. Upon drying in an oven at 50 ^oC for 2 h, the electrode was covered with 5.4 μL of 0.05 wt% Nafion. Cyclic voltammograms (CVs) of the NPs were

obtained in Ar-purged 0.1 M $HClO_4$ and 0.1 M $HClO_4$ containing 2.0 M CH_3OH or 2.0 M HCOOH with a scan rate of 50 mV s^{-1} at 25 °C. For comparison of electrocatalytic stability, the NPs were kept at 0.45 V for 7200 s in Ar-purged 0.1 M $HClO_4$ containing 2.0 M CH_3OH or 2.0 M HCOOH.

3. Results and discussion

The PtPd NPs synthesized in the presence of $Mo(CO)_6$ are shown in the TEM images in Fig. 2a. The PtPd NPs showed an average size of ~11.9 nm and a yield of cubic shape (denoted as cubic PtPd) of ~92.4% (Fig. 2b). Fig. 2c shows a high-resolution TEM (HR-TEM) image of a single c-Pt-Pd NP grown along {100} crystal planes. The fast Fourier-transform (FFT) pattern indicates that the c-Pt-Pd NP is a single crystal with its surface enclosed by {100} facets (Fig. 2d). The cubic PtPd NPs represent the {100} facets with d-spacing of 0.196 nm of Pt-Pd metallic phase based on a face-centered cubic (fcc) structure. Furthermore, the Pt NPs synthesized using a thermal decomposition method in the presence of $Mo(CO)_6$ showed an average size of ~13.5 nm and a yield of cubic shape (denoted as cubic Pt) of ~74.0% (Fig. 2e and f). The cubic Pt NPs were grown along {100} crystal planes with d-spacing of 0.198 nm of Pt metallic phase (Fig. 2g and h). In contrast, the PtPd NPs synthesized in the absence of $Mo(CO)_6$ showed an irregular shape with an average size of ~10.6 nm (Fig. 2i-l). To clarify the effect of metal hexacarbonyl, PtPd NPs were prepared using a thermal decomposition method in the presence of $W(CO)_6$. The as-prepared PtPd NPs exhibited an average size of ~12.5 nm and a yield of cubic shape of ~92% (Fig. S1a and b). The high-resolution HR-TEM image and FFT pattern of the PtPd NP indicate a single crystal grown along {100} facets (Fig. S1c and d), which is in agreement with the result synthesized in the presence of $Mo(CO)_6$. This implies that the metal carbonyls such as $Mo(CO)_6$ and $W(CO)_6$ during the chemical synthesis of metallic NPs can assist the formation of the cubic shape. For comparison, the polycrystalline PtPd alloy NPs (denoted as poly-PtPd) were prepared using a borohydride reduction method, as shown in Fig. S1e-h. The as-prepared poly-PtPd exhibited an irregular shape with an average size of ~5.0 nm.

Fig. 3a shows wide-range XRD patterns of the as-prepared NPs. The XRD patterns of the PtPd and Pt NPs contain diffraction peaks corresponding to (111), (200) and (220) of a typical fcc crystal structure. No diffraction signal of pure Pd or pure Mo was observed from the XRD patterns, indicating that a single Pt-based phase was formed through the chemical process. In particular, assuming a substitutional solid solution between metallic Pt and Pd, since the radius of the Pt atom (0.139 nm) is greater than the radius of the Pd atom (0.137 nm), the higher angle shift of the XRD peaks for the cubic PtPd NPs indicates

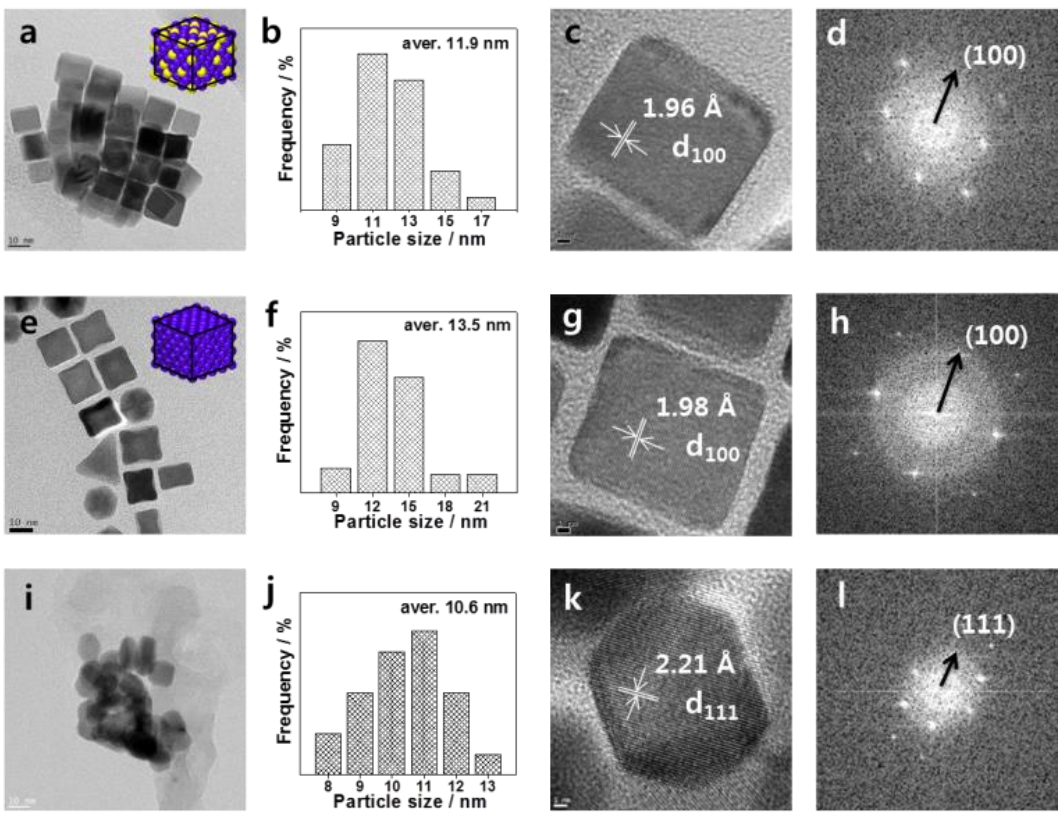

Fig. 2 HR-TEM images, size distribution histograms, high-resolution TEM images, and FFT patterns of the cubic PtPd ((a)-(d)) and cubic Pt ((e)-(h)) synthesized in the presence of $Mo(CO)_6$, and PtPd ((i)-(l)) NPs synthesized in the absence of $Mo(CO)_6$

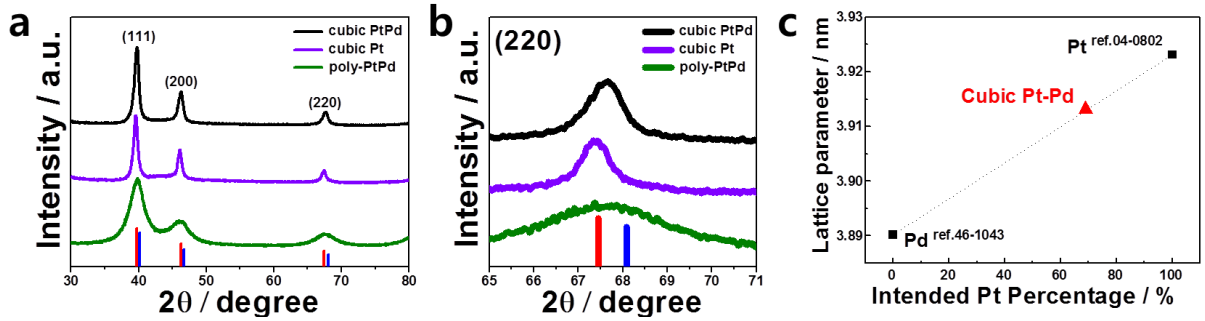

Fig. 3 (a) Wide and (b) fine scan XRD patterns of the as-prepared NPs compared to the reference data of pure Pt and Pd metallic phases. (c) Plot of lattice parameter versus Pt atomic percentage of the cubic PtPd NPs.

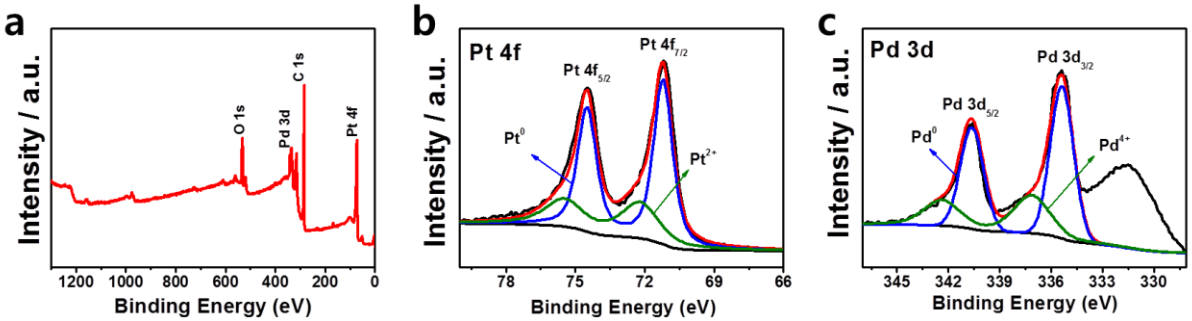

Fig. 4 (a) Wide-scan XPS spectrum, (b) Pt 4f, and (c) Pd 3d spectra for the cubic PtPd NPs

an alloy formation between Pt and Pd. As shown in Fig. 3b, the XRD peak in the cubic PtPd NPs was shifted into a higher 2θ value of 0.21° in a (220) diffraction peak. Based on the Vegard's law of $d_{PtPd} = X \cdot d_{Pt} + (1\text{-}X) \cdot d_{Pd}$, the atomic composition of Pt and Pd in cubic PtPd NPs is 69.0 and 31.0 at%, respectively. The lattice parameter of the cubic PtPd NPs reflecting the degree of alloying in the bimetallic structure is indicated in Fig. 3c. The lattice parameter of the cubic PtPd NPs appeared on a straight fitted line based on a solid solution between Pt and Pd, which means a well-defined alloy formation. The surface chemical states and composition of elemental components in the cubic PtPd NPs were characterized using XPS analysis. Typically, the Pt $4f_{7/2}$ and $4f_{5/2}$ peaks appear at ~71 and ~73 eV, respectively, with the theoretical area ratio of 4:3. Furthermore, the Pt 4f peaks in the cubic PtPd NPs consist of metallic and oxide states i.e., the peaks for Pt^0 and Pt^{2+} at ~71.1 and ~72.3 eV, respectively (Fig. 4b). The Pd $3d_{5/2}$ and $3d_{3/2}$ peaks typically appear at ~335 and ~340 eV, respectively, with the theoretical area ratio of 3:2. The Pd 3d peaks in the cubic PtPd NPs consist of metallic and oxide states; i.e., the characteristic peaks for Pd^0 and Pd^{4+} at 335.4 and 340.6 eV, respectively (Fig. 4c). The elemental compositions for the cubic PtPd NPs measured using XPS are 69.5 at% of Pt and 30.5 at% of Pd. By comparing the EDX, XRD, and XPS data, it was found that the cubic PtPd NPs exhibited a homogeneous distribution of Pt and Pd atoms in both the bulk and surface of the cubic NPs, as shown in Fig. S2. As a result, it can be concluded that the cubic PtPd NPs prepared by the present synthetic process have a well-defined alloy nanostructure with {100} facets of an fcc structure.

In general, it was reported that Pt nanostructures could expose the most stable face such as {100}, {110}, or {111} under a particular condition of a chemical synthesis process. Moreover, among the stable faces, the exposed face could be selected by modulating the growth rate of Pt nanostructures. Especially, it is most likely that a nanostructure with a particular face is selectively formed due to a slow growth rate during the process with chemical environments. This demonstrates that the kinetics of nucleation and the growth of NPs in homogeneous solutions can be adjusted by the controlled release of anions, cations, and surfactants. Thus, to facilitate the growth of cubic Pt-based NPs in the present synthetic condition, the {100} surfaces should have the lowest

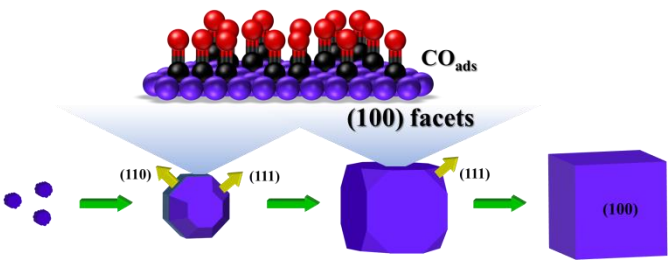

Fig. 5 Schematic illustration of formation mechanism of the cubic PtPd NPs synthesized in the presence of $Mo(CO)_6$ or $W(CO)_6$.

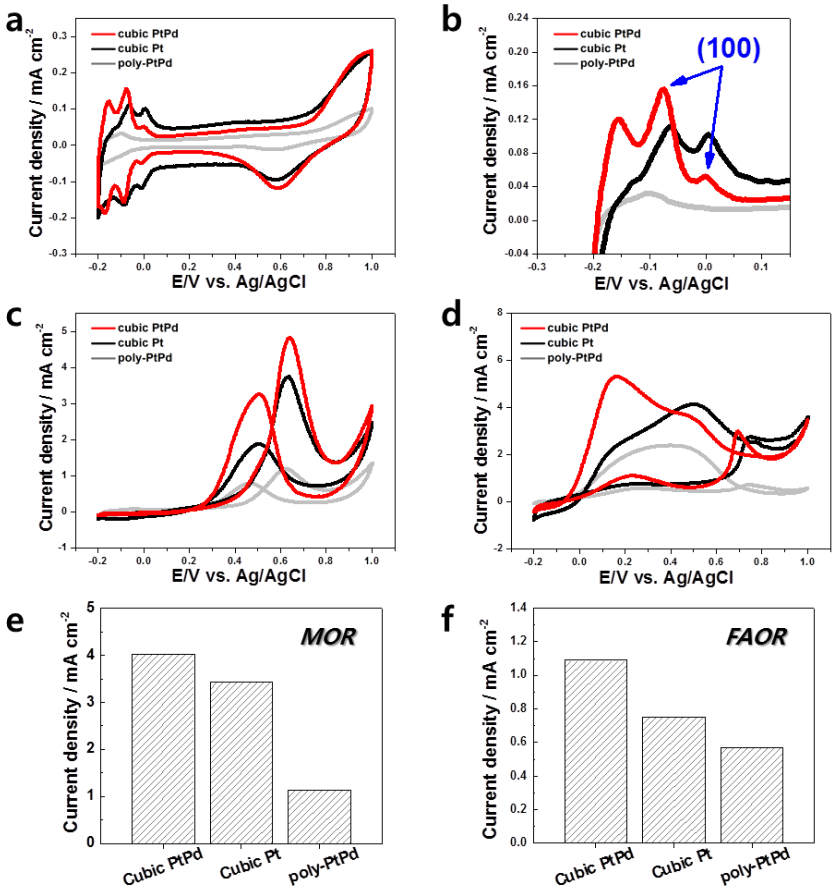

Fig. 6 (a) CVs and (b) hydrogen desorption regions of the as-prepared NPs in Ar-saturated 0.1 M $HClO_4$ with a scan rate of 50 mV s^{-1} at 25 °C. CVs of the as-prepared NPs for (c) MOR and (d) FAOR in 0.1 M $HClO_4$ + 2.0 M CH_3OH and 0.1 M $HClO_4$ + 2.0 M HCOOH, respectively, at 25 °C. Comparison of oxidation current densities of the as-prepared NPs for (e) MOR and (f) FAOR at 0.60 and 0.23 V, respectively.

surface energy. The surface selective capping agents could alter the morphology of NPs by lowering the binding energy on the {100} surfaces of PtPd NPs. Here, in particular, the PtPd cubes prepared using a thermal decomposition method in the presence of $Mo(CO)_6$ presented the crystal plane of {100} of an fcc crystal structure. During the chemical process for the PtPd cubes, the Mo^{n+} greatly reduced the supersaturation of Pt and Pd atoms,[37] thus forming a stable crystal plane, as in the following equation:

$$Mo^0 + 3Pt^{2+}(Pd^{2+}) \rightarrow Mo^{6+} + 3Pt^0(Pd^0)$$

As illustrated in Fig. 5, the carbon monoxide generated from the metal carbonyls during the synthesis was more favorably adsorbed on {100} than the other faces.[38] As a result, the highly selective growth of cubic PtPd NPs with the exposure of thermodynamically stable {100} faces is believed to be due to the relatively low redox potential of Mo^{n+} and favorable binding of CO on {100} Pt-based surfaces.

To identify the electrochemical properties of the electrocatalysts, CVs were obtained in Ar-saturated 0.1 M $HClO_4$ with a scan rate of 50 mV s^{-1} at 25 °C (Fig. 6a and b). The {100} surfaces with a small coordination number for the cubic PtPd NPs exhibited particularly electrochemical adsorption and desorption properties of hydrogen and oxygen.[39] The cubic PtPd NPs with dominant {100} facets show a first oxidation current peak at around -0.076 V vs. Ag/AgCl and dominant second peak at around 0.0 V for hydrogen desorption. Similarly, the cubic Pt NPs with dominant {100} facets shows a first oxidation current peak at around -0.063 V vs. Ag/AgCl and second peak at around 0.005 V for hydrogen desorption. According to the previous electrochemical results on Pt single crystals, this demonstrates that the Pt cube as an electrocatalyst dominantly possesses {100} rather than {111} faces, which is in good agreement with the TEM results. On the other hand, in the case of the poly-PtPd NPs, the CV shows a voltammetric profile characteristic of a poly-oriented surface. It was reported that the Pt-Pd alloy represented a mixed adsorption and desorption peak of underpotentially deposited hydrogen between the Pt and Pd surfaces.[40] The CVs of the as-prepared samples for MOR and FAOR were obtained in 0.1 M $HClO_4$ + 2.0 M CH_3OH and 0.1 M $HClO_4$ + 2.0 M HCOOH at 25 °C (Fig. 6c and d). Theoretically, the MOR and FAOR can proceed

at -0.164 and -0.46 V vs. Ag/AgCl, respectively, as the following equations of $CH_3OH + H_2O \rightarrow CO_2 + 6H^+ + 6e^-$ and $HCOOH \rightarrow CO_2 + 2H^+ + 2e^-$, respectively.[41,42] Thus, a lower onset potential implies evidence of a superior electrocatalytic activity for electrooxidation reactions. In particular, the cubic PtPd NPs exhibited lower onset potentials for MOR and FAOR, indicating excellent electrocatalytic activity compared to the cubic Pt and poly-PtPd NPs. Moreover, the oxidation current densities of 4.10 and 1.09 mA cm^{-2} of the cubic PtPd NPs for MOR and FAOR at 0.60 and 0.23 V, near the kinetically controlled potentials, respectively, exceeded those for the cubic Pt and poly-PtPd NPs (Fig. 6e and f).

To evaluate electrocatalytic stability for MOR and FAOR, the NPs were maintained at 0.45 V for 7200 s in 0.1 M $HClO_4$ + 2.0 M CH_3OH and 0.1 M $HClO_4$ + 2.0 M HCOOH, respectively, at 25 °C.[16,44] The cubic PtPd NPs exhibited much higher current densities and thus slight current reduction ratios of 23% and 13%, after the stability test of MOR and FAOR, respectively (Fig. S3). In contrast, in the case of the cubic Pt and poly-PtPd NPs, the current density after the stability test decreased significantly, representing the considerable reduction ratios from the initial values. After the stability test of oxidation reactions, the variation of morphology and size for the NPs as catalysts could affect the electrocatalytic properties for MOR and FAOR. As a result, the cubic PtPd NPs with highly improved activity and stability for MOR and FAOR due to both the well-defined cubic nanostructure and homogeneous distribution of Pt and Pd atoms may be utilized as a promising anode in fuel cell applications. However, since the large particle size of the NPs might limit their practical application as electrocatalysts in fuel cells, the downsizing of the cubic NPs should be carried out as a further work.

4. Conclusions

In summary, we synthesized the cubic PtPd alloy NPs for electro-oxidation reactions of methanol and formic acid using a thermal-decomposition method in the presence of $Mo(CO)_6$. In particular, the PtPd NPs presented a dominant {100} face of an fcc structure and well-defined alloy formation between the Pt and Pd metallic phases. The thermodynamically stable {100} exposure of the PtPd NPs might result from the slow nucleation and selective growth caused by Mo^{n+} and CO. The improved electrochemical properties of the cubic PtPd NPs for methanol and formic acid electro-oxidation may be attributed to dominant {100} facets with a well-defined PtPd alloy formation between metallic phases.

Acknowledgements

This work was supported by the National Research Foundation of Korea Grant funded by the Korean Government (NRF-2013R1A1A2012541).

Notes and references

[a] Department of Chemical Engineering, Soongsil University, Seoul 156743, Republic of Korea
[b] Department of Engineering Science, University of Oxford, Oxford OX1 3PJ, United Kingdom

† Electronic Supplementary Information (ESI) available: Additional HRTEM, EDX, XRD, XPS, and CV data.

1 Y.-W. Lee and K.-W. Park, *Catal. Comm.*, 2014, **55**, 24-28.
2 L. Wang and Y. Yamauchi, *Chem. Mater.*, 2011, **23**, 2457-2465.
3 Q. Lv, Y. Xiao, M. Yin, J. Ge, W. Xing and C. Liu, *Electrochim. Acta*, 2014, **139**, 61-68.
4 J. Xu, Y. C. Liu, Y. Zhou, T. Lu and Y. Tang, *J. Mater. Chem.*, 2012, **22**, 23659-23667.
5 J.-N. Zheng, L.-L. He, C. Chen, A.-J. Wang, K.-F. Ma and J.-J. Feng, *J. Power Sources*, 2014, **268**, 744-751.
6 J.-M. Yoon, J.-W. Lee, H.-G. Lee and Y.-T. Yu, *Int. J. Electrochem. Sci.*, 2014, **9**, 5690-5698.
7 O. Sahin and H. Kivrak, *Int. J. Hydrogen Energy*, 2013, **38**, 901-909.
8 O. Guillén-Villafuerte, R. Guil-López, E. Nieto, G. García, J. L. Rodríguez, E. Pastor and J. L. G. Fierro, *Int. J. Hydrogen Energy*, 2012, **37**, 7171-7179.
9 C. He, H. R. Kunz and J. M. Fenton, *J. Electrochem. Soc.*, 2003, **150**, A1017-A1024.
10 W. Xu, T. Lu, C. Liu and W. Xing, *J. Phys. Chem. B*, 2005, **109**, 14325-14330.
11 H. A. Gasteiger, N. M. Marković and P. N. Ross, *J. Phys. Chem.*, 1995, **99**, 8290-8301.
12 D. C. Papageorgopoulos, M. Keijzer, J. B. J. Veldhuis and F. A. de Bruijn, *J. Electrochem. Soc.*, 2002, **149**, A1400-A1404.
13 J.-H. Choi, K.-W. Park, I.-S. Park, K. Kim, J.-S. Lee and Y.-E. Sung, *J. Electrochem. Soc.*, 2006, **153**, A1812-A1817.
14 H. Zhang, M. Jin, H. Liu, J. Wang, M. J. Kim, D. Yang, Z. Xie, J. Liu and Y. Xia, *ACS Nano*, 2011, **5**, 8212-8222.
15 B. T. Sneed, A. P. Young, D. Jalalpoor, M. C. Golden, S. Mao, Y. Jiang, Y. Wang and C.-K. Tsung, *ACS Nano*, 2014, **8**, 7239-7250.
16 X. Yu and P. G. Pickup, *J. Power Sources*, 2008, **182**, 124-132.
17 L. Zhang, Y. Tang, J. Bao, T. Lu and C. Li, *J. Power Sources*, 2006, **162**, 177-179.
18 X. Wang, Y. Tang, Y. Gao and T. Lu, *J. Power Sources*, 2008, **175**, 784-788.
19 C. Rice, S. Ha, R. I. Masel, P. Waszczuk, A. Wieckowski and T. Barnard, *J. Power Sources*, 2002, **111**, 83-89.
20 C. Rice, S. Ha, R. I. Masel and A. Wieckowski, *J. Power Sources*, 2003, **115**, 229-235.
21 N. M. Marković, H. A. Gasteiger and P. N. Ross, *Electrochim. Acta*, 1995, **40**, 91-98.
22 Y.-H. Cho, O.-H. Kim, D. Y. Chung, H. Choe, Y.-H. Cho and Y.-E. Sung, *Appl. Catal. B-Environ.*, 2014, **154-155**, 309-315.
23 T. S. Ahmadi, Z. L. Wang, T. C. Green, A. Henglein and M. A. El-Sayed, *Science*, 1996, **272**, 1924-1926.
24 X. Liu, W. Wang, H. Li, L. Li, G. Zhou, R. Yu, D. Wang and Y. Li, *Sci. Rep.*, 2013, **3**, 1404.
25 C. Cui, L. Gan, M. Heggen, S. Rudi and P. Strasser, *Nature Mater.*, 2013, **12**, 765-771.

26 S.-I. Choi, S. Xie, M. Shao, J. H. Odell, N. Lu, H.-C. Peng, L. Protsailo, S. Guerrero, J. Park, X. Xia, J. Wang, M. J. Kim and Y. Xia, *Nano Lett.*, 2013, **13**, 3420-3425.
27 M. Shao, G. He, A. Peles, J. H. Odell, J. Zeng, D. Su, J. Tao, T. Yu, Y. Zhu and Y. Xia, *Chem. Commun*., 2013, **49**, 9030-9032.
28 J. Chen, B. Lim, E. P. Lee and Y. Xia, *Nano Today*, 2009, **4**, 81-95.
29 Y. Xia, Y. Xiong, B. Lim and S. E. Skrabalak, *Angew. Chem. Int. Ed.*, 2009, **48**, 60-103.
30 Y. Qi, T. Bian, S.-I. Choi, Y. Jiang, C. Jin, M. Fu, H. Zhang and D. Yang, *Chem. Commun.*, 2014, **50**, 560-562.
31 X. Huang, Z. Zhao, J. Fan, Y. Tan and N. Zheng, *J. Am. Chem. Soc.*, 2011, **133**, 4718-4721.
32 N. S. Porter, H. Wu, Z. Quan and J. Fang, *Acc. Chem. Res.*, 2013, **46**, 1867-1877.
33 C. Kim and H. Lee, *Catal. Comm.*, 2009, **10**, 1305-1309.
34 E. S. Steigerwalt, G. A. Deluga and C. M. Lukehart, *J. Phys. Chem. B*, 2002, **106**, 760-766.
35 T. H. M. Housmans, A. H. Wonders and M. T. M. Koper, *J. Phys. Chem. B*, 2006, **110**, 10021-10031.
36 Y. Kang and C. B. Murray, *J. Am. Chem. Soc.*, 2010, **132**, 7568-7569.
37 J. Zhang and J. Fang, *J. Am. Chem. Soc.*, 2009, **131**, 18543-18547.
38 G. Chen, Y. Tan, B. Wu, G. Fu and N. Zheng, *Chem. Commun.*, 2012, **48**, 2758-2760.
39 H. Yang, L. Dai, D. Xu, J. Fang and S. Zou, *Electrochim. Acta*, 2010, **55**, 8000-8004.
40 Y.-W. Lee, S.-E. Oh and K.-W. Park, *Electrochem. Comm.*, 2011, **13**, 1300-1303.
41 M. Neurock, M. Janik and A. Wieckowski, *Faraday Discuss.*, 2008, **140**, 363-378.
42 S. Zhang, S. GuO, H. Zhu, D. Su and S. Sun, *J. Am. Chem. Soc.*, 2012, **134**, 5060-5063.
43 T. Iwasita, *Electrochim. Acta*, 2002, **47**, 3663-3674.